構成・システム生物学　（豊田担当分）　レポート課題

2015.12.8

問１．平衡状態におけるジャイアントベシクルの形状について，膜の弾性エネルギーの観点から Area Difference Elasticity モデルが提案されている。このモデルにより，次のような相図（図中の図形はジャイアントベシクルの断面図であり、starfish 以外は回転体である）が導かれる。

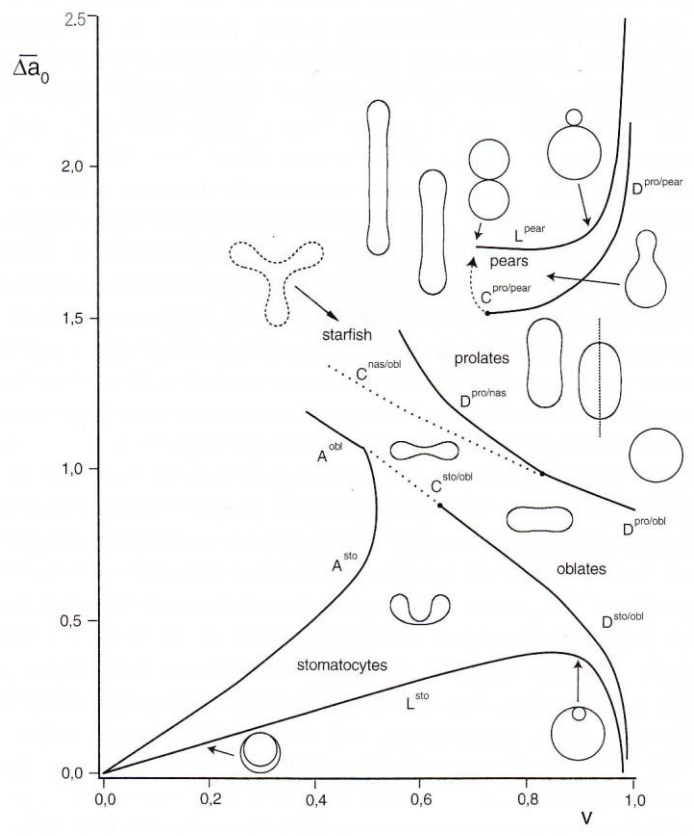

出典　P.L.Luisi,P.Walde eds. *Giant Vesicles*, John.Wiley.&Sons,2000,p.157

＜提出締切日＞

2016 年 1 月 12 日（火）

＜提出先＞

16 号館 604 室扉　提出 BOX

横軸は，規格化された体積（$v := V/\{(4\pi/3)(A/4\pi)^{3/2}\}$，$V$は体積, A は表面積）であり，縦軸は 2 分子膜内外の膜の実効的な表面積差（$\overline{\Delta a_0}$）である。

このモデルに従ってジャイアントベシクルが形態変化すると仮定すると，

(i)　ジャイアントベシクルが球（$v = 1.0$、$\overline{\Delta a_0} = 1.0$）から 2 つの連結した球へ形態変化するには，内部の水の体積（分子数）及び内外の膜の表面積（膜分子の数）がどのように変化すると考えられるか説明せよ。

(ii)　球形のジャイアントベシクルがもとと同じ大きさの 2 つの球形（連結されたままでよい）へ形態変化するには，内部の水の体積（分子数）及び内外の膜の表面積（膜分子の数）がどのように変化すると考えられるか説明せよ。

問２．ポリスチレンの微粒子を内包したジャイアントベシクルの形態変化に関する論文（Y. Natsume et al., *Soft Matter*, **2010**, *6*, 5359–5366）を読み，2000 字程度で要約しなさい。適宜，式や図を含めてもよい（それらの中の文字については字数としてカウントしない）。

＊資料は http://park.itc.u-tokyo.ac.jp/toyota_lab/researches.html からダウンロードできる。

以上。

Shape deformation of giant vesicles encapsulating charged colloidal particles

Yuno Natsume,†[a] Olivier Pravaz,‡[a] Hirohisa Yoshida[b] and Masayuki Imai*[a]

Received 19th May 2010, Accepted 6th August 2010
DOI: 10.1039/c0sm00396d

We have investigated shape deformations of giant vesicles induced by the confinement of charged colloids. By confining charged colloids densely, the non-spherical vesicles with tube, discocyte, and stomatocyte shapes transformed to multi-bead vesicles composed of *n* spheres. The size and number of spheres in the multi-bead vesicle are determined by a conservation law of the total volume and area. The morphology transition of the vesicle induced by the charged colloid confinement is caused by the optimization of the free volume of the confined charged colloids in a vesicle.

Introduction

Soft matter forms characteristic mesoscopic structures, which are stabilized by a delicate balance between the entropic and the enthalpic interactions. By doping guest particles, the additional entropic or enthalpic interaction between the guest particle and the host mesoscopic structure induces structural transitions. The most familiar entropic interaction induced by the guest particles is the depletion interaction,[1–3] which was first recognized in the sphere/polymer mixtures and then observed in various soft matter complex systems, such as rod/polymer and rod/spherical colloid mixtures.[1,4–10] In these systems, the guest particles obtain large free volume by overlapping the depletion zone surrounding the host particles. The increase of the free volume raises the translational entropy of guest particles, but at the expense of lowering the entropy of mixing. If the gain in free volume is sufficient, the host particles aggregate, *i.e.* the effective attractive interaction between the host particles. This concept is easily extended to more complicated systems, membrane/polymer.[11–15] By confining neutral polymer chains between lamellar membranes, the opposing membranes overlap their depletion zones to obtain the large free volume for the guest polymer chains. This effective attractive inter-lamellar interaction (depletion interaction) destabilizes the lamellar membranes and finally causes a phase separation into a dilute lamellar phase where the polymer chains are localized in and a concentrated lamellar phase as shown by Ligoure *et al.*[13–15] On the other hand, when one confines colloids between the lamellar membrane slits, the colloids suppress the fluctuation of lamellar membranes, which leads an effective repulsive interaction between membranes.[16–20] The suppression of membrane fluctuations causes a morphological transition from lamellar membranes to worm-like micelles to release the geometrical frustration.[20]

The structural transitions induced by the guest particles might be more emphasized, when the guest particles are confined into a closed capsule. In this context, we confined water-soluble polymer chains (gelatin) inside of nanometre-sized water droplets of microemulsion.[21] By confining polymer chain in nanometre-sized droplet, spherical droplets changed to prolate droplets due to a loss of the conformational entropy of polymer chains or a specific interaction between surfactant monolayer and gelatin. In this study we investigate a simple confinement system, where we confine charged colloidal particles inside of a giant vesicle (GV) having micrometre size. The shape of the GV encapsulating colloids is determined by the minimization of the total free energy, F_t, expressed by

$$F_t = F_m + F_c \quad (1)$$

under the geometrical constraints, fixed vesicle volume, V, and fixed surface area, A. The first term, F_m, means the membrane elastic energy of a vesicle and may be appropriate to adopt an area difference elasticity (ADE) model[22–24] composed of the bending energy and ADE energy contributions given by

$$F_m = \frac{1}{2}\kappa \int (2H)^2 \, dS + \frac{\alpha\pi\kappa}{2At^2}(\Delta A - \Delta A_0)^2 \quad (2)$$

The bending energy term is expressed by the bending rigidity, κ, and the mean curvature, H. The ADE term arises from the deviation in the actual area difference between the inner and the outer leaflets of the bilayer, $\Delta A = 2t\oint H dA$, from the intrinsic area difference, ΔA_0, where t is the distance between two monolayers. The intrinsic area difference is defined by $\Delta A_0 = (N_{out} - N_{in})s_0$, where s_0 is the cross-section of a lipid molecule and N_{out} and N_{in} correspond to the numbers of lipids in outer and inner leaflets, respectively. The prefactor is expressed using the total membrane area, A, and a numerical constant, α, which decides the relative strength of the ADE energy compared to the bending energy. The second term, $F_c(N, V_f, T)$, represents the free energy of confined charged colloids[25–27] (radius a and total number of colloids N) with the electrostatic repulsive interaction. Thus this term requests largest free volume for confined colloids. Since the colloidal particles are confined in a vesicle with volume V, the effective free volume for the colloidal particles, V_f, is expressed by $V_f = V - V_{dep}$, where V_{dep} is the volume of the depletion zone covering the inside of the vesicle

[a]*Department of Physics, Ochanomizu University, 2-1-1 Otsuka, Bunkyo, Tokyo, 112-8610, Japan. E-mail: imai@phys.ocha.ac.jp*
[b]*Department of Applied Chemistry, Tokyo Metropolitan University, 1-1 Minami-Osawa, Hachioji, Tokyo, 192-0397, Japan*
† Present address: Department of Basic Science, Graduate School of Arts and Sciences, The University of Tokyo, 3-8-1 Komaba, Meguro, Tokyo, 153-8902, Japan.
‡ Present address: Adolphe Merkle Institute, University of Fribourg, Rte de l'Ancienne Papeterie, P.O. Box 209, CH-Marly 1, Switzerland.

membrane with the thickness a (colloid radius). Under the geometrical constraints, the elastic energy term, F_m, leads to various vesicle shapes, such as oblate, prolate, stomatocyte and starfish, whereas the confined colloid term, F_c, prefers the vesicle shape giving the maximum free volume. The competition between the two terms brings a shape deformation characteristic to the vesicle encapsulating colloidal particles.

Experimental

Reagents

We prepared GVs composed of DOPC (1,2-dioleoyl-*sn*-glycero-3-phosphocholine). DOPC (>99% purity) was obtained in a powder form from Avanti Polar Lipid (Alabaster, AL, USA) and used without further purification. Texas-Red dihexanoylphosphatidylethanolamine (TR-DHPE) was obtained from Molecular Probes (Eugene, OR, USA), and used as a dye for the fluorescence microscope observation. In lipid film formation by a gentle hydration method,[28] we added D(+)-glucose (Glc) obtained from AppliChem GmbH (Darmstade, Germany). We used fluorescent polystyrene latex with the diameter of 1 μm (Fluoresbrite caboxy YG 1.0 microspheres with excitation max. = 441 nm and emission max. = 486 nm) purchased from Polysciences, Inc. (Warrington, PA, USA) as the confined colloidal particles. In order to remove the excess surfactants and impurities the latex suspension was dialyzed using cellulose tubes with the pore size of 40–50 Å (Viskase Companies Inc., IL, USA) against purified water for about two weeks. The completeness of the dialysis was verified by adsorption spectrum measurements in the region of 200–1100 nm. We confirmed by eye observations that the dialysis did not induce the aggregation of the colloidal particles. After the dialysis the ζ-potential of the colloids in 0.1 mM Glc solution was −37 mV. The ζ-potential was obtained by electrophoretic mobility (based on Smoluchowski model) from the colloidal suspension using ELSZ2 (Otsuka Electronics, Hirakata, Japan).

Preparation of GVs encapsulating colloids

We prepared GVs encapsulating colloids by the following procedure based on an efficient gentle hydration technique.[28] First we dissolved DOPC in chloroform at a concentration of 2 mM and then TR-DHPE was added to the chloroform solution with a mole ratio of 0.01 : 1 (dye : DOPC). Glc was dissolved in methanol at a concentration of 2.5 mM. The DOPC solution was diluted with pure chloroform to a concentration of 0.125 mM and then the 800 μl of 0.125 mM DOPC solution and 400 μl of 2.5 mM of Glc solution were mixed in a clean glass tube. The tube was homogenized using a vortex mixer at room temperature. The solvent was evaporated in a stream of nitrogen gas and the obtained lipid film was kept under vacuum for 1 night to remove the remaining solvent completely. We added 30 μl of 0.2% colloidal suspension at 25 °C. After 2–3 minutes of prehydration, the sample was hydrated with 970 μl of the colloidal suspension at 25 °C. In order to obtain GVs encapsulating dense colloids (GEDC), we performed the hydration under centrifugation. By the centrifugation, colloids were sedimented at the bottom of the tube, where the lipid films spontaneously formed vesicles. We performed centrifugation with 1500 rpm at 25 °C (Sorvall Biofuge PrimoR: Kendro, Germany). The obtained GVs encapsulated dense colloidal particles at the colloid volume fraction of $\phi_v \cong 0.5$. The volume fraction was estimated from the area fraction of colloids inside of a vesicle, ϕ_A, by assuming the isotropic distribution of the encapsulating colloids, *i.e.* $\phi_v = \frac{1}{L}\int_0^L \phi_A dz = \phi_A$, where z is the coordinate normal to the area and L is the height of the sampling volume.

Fluorescence microscope observation

The vesicle suspension was put on a glass plate with a silicon rubber spacer having the thickness of 0.5 mm. The shape deformation of GV encapsulating colloids was followed using a two-color confocal fluorescence microscope with a He–Ne laser (543 nm) and a Ar laser (488 nm) (LSM 5, Carl Zeiss, Germany). The GV membranes dyed by TR-DHPE show red color, while the fluorescent colloids show yellow color, which make it easy to observe the shape deformations of GV encapsulating colloids. To avoid photo-oxidation, we minimized the exposure to light.

Surface pressure *versus* molecular area isotherm

In order to examine the adsorption of lipids on the colloid surface, we measured surface pressure *versus* molecular area (π–A) isotherms. The π–A isotherms were recorded on a Langmuir–Blodgett film deposition apparatus (NL-LB 240S-MWC, Filgen Inc., Nagoya, Japan) using a moving wall method. The trough was enclosed in a thermostated box. The temperature was regulated to 23.5 ± 0.5 °C. To examine the adsorption, we equilibrated DOPC lipids (2.01×10^{-7} mol) in 2 ml colloidal suspension with the colloid volume fraction of $\varphi_v = 0$, 0.02, and 0.10. By assuming that the cross-section area of a DOPC molecule is 0.725 nm,[2,29] the ratios of total cross-section area of the DOPC lipids (Σ_{DOPC}) to the total surface area of the colloids (Σ_{col}) in the suspension were $\Sigma_{col}/\Sigma_{DOPC} = 0$, 2.6, and 13 for $\varphi_v = 0$, 0.02, and 0.10 respectively. We sampled 100 μl of the equilibrate suspension and deposited the sample on pure water in the trough for the surface pressure measurements. The spread lipid layer was compressed at constant rate of 5 cm^2 min^{-1} to obtain the π–A isotherm. We measured the surface pressure–area isotherms five times for each sample and confirmed that the accuracy of the onset area is within ±3%.

Results

Shape deformation of GVs encapsulating colloids

First we show the effect of the colloid confinement on the vesicle shape briefly. As mentioned in Introduction section, the vesicle shape is determined by optimizing the total free energy under the geometrical constraints. Here we introduce a measure of the geometrical constraints, excess area, ξ, defined by

$$\xi \equiv (A/4\pi)^{1/2}/(3V/4\pi)^{1/3} - 1 \quad (3)$$

We demonstrate the shape deformations of vesicles induced by the excess area in Fig. 1. Fig. 1(a) shows GVs without colloids just after the hydration, where membranes are designated by red color. In this case most of GVs have spherical shape with

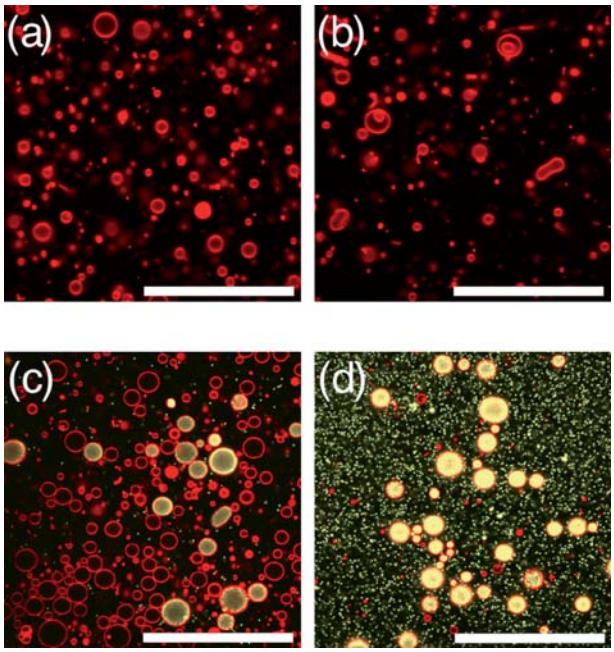

Fig. 1 Effect of confinement of colloids on GV morphology. Shape deformation of GVs without colloids: (a) just after hydration and (b) 60 min after addition of a solute (4 mM). Shape deformation of GVs encapsulating dense colloids: (c) just after hydration and (d) 30 min after addition of a solute (0.9 mM). Membranes and colloids are designated by red and white colors, respectively. Scale bar in each figure indicates 100 μm.

$\xi \cong 0$ and the spherical vesicle shape was independent of time due to the geometrical constraints. Then we added a solute, sorbitol (4 mM), to the GV suspension, which causes the osmotic pressure difference between inside and outside of the GV. With elapse of time, the volume of the vesicle decreases with keeping the membrane area constant, which results in the increase of the excess area.[30,31] Using the excess area, the spherical GVs deform into prolate, oblate and stomatocyte shapes as shown in Fig. 1(b).

When we confined colloidal particles inside of the GV sparsely ($\varphi_v < 0.03$), vesicles showed the similar shape deformations to those without colloids. Thus we could not observe a definite effect of the confinement of colloids on the GV morphology. On the other hand, when we hydrated the lipid film under the centrifugation, some of spherical GVs encapsulated many colloids and the volume fraction of colloids, φ_v, is approximately 0.5 as shown in Fig. 1(c), where colloids are designated by white color. The spherical GV encapsulating dense colloids (GEDCs) kept the shape constant due to the geometrical constraint, $\xi \cong 0$. Again we introduced the excess area to the GEDCs by applying the osmotic pressure difference (sorbitol 0.9 mM). The GEDCs transformed to twins, triplets, or multi-bead necklaces as shown in Fig. 1(d) and we never observed stable prolate, oblate, and stomatocyte GEDCs, which are stable shapes in GVs without dense colloids (Fig. 1(b)). Boroske *et al.* showed that the osmotic pressure difference between outside and inside vesicle induces a lipid flow, which results in the formation of submicroscopic daughter vesicles.[32] In our study to estimate the effect of the osmosis on the vesicle morphology, we examined vesicle deformations induced by pure osmotic pressure difference without colloids (Fig. 1(a) and (b)). Without colloids, we hardly observed the twin vesicle formation, indicating that the encapsulated colloids are responsible for the twin vesicle formation. These results indicate that by confining the charged colloids inside of the vesicle densely, the vesicle show a new shape deformation pathway.

Fig. 2(a) shows a shape deformation pathway of a spherical GEDC induced by applying the osmotic pressure difference. By adding the solute, a spherical GEDC started to fluctuate between oblate and prolate shapes (<600 s), and then transformed to the tubular shape (690 s). With elapse of time, the tubular vesicle deformed to a twin vesicle connected by a narrow neck (1120 s). We estimated the change of the excess area during this shape deformation process by assuming that the vesicle has an axisymmetry shape.

Here we mention how to estimate the key parameter ξ, from the 2D vesicle images. In this study we focused on four vesicle

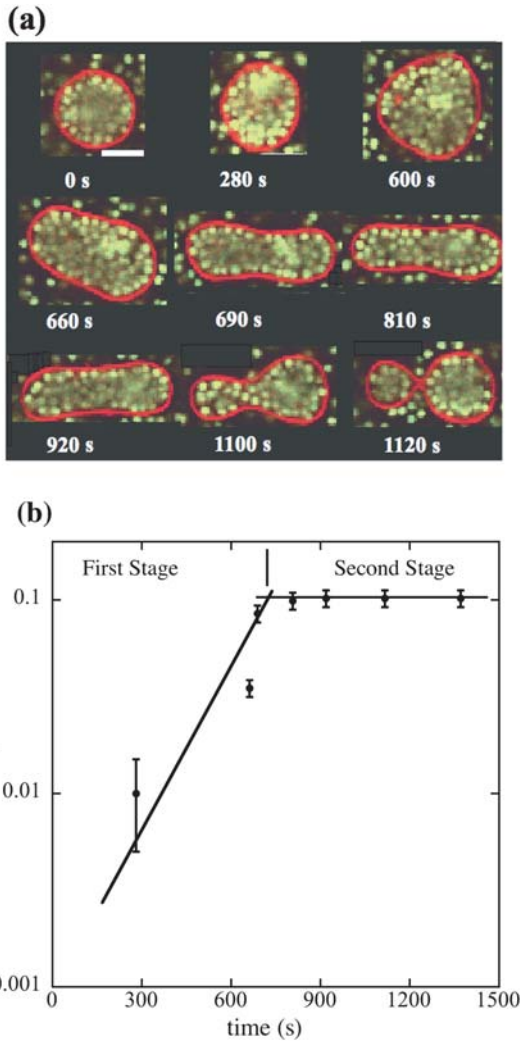

Fig. 2 Shape deformation pathway of GEDC induced by applying osmotic pressure difference between inside and outside of the vesicle. (a) Time evolution of vesicle deformation from a sphere to a twin vesicle and (b) change of the excess area, ξ, during the deformation pathway. Scale bar in (a) indicates 5 μm and other photos in (a) have the same scale.

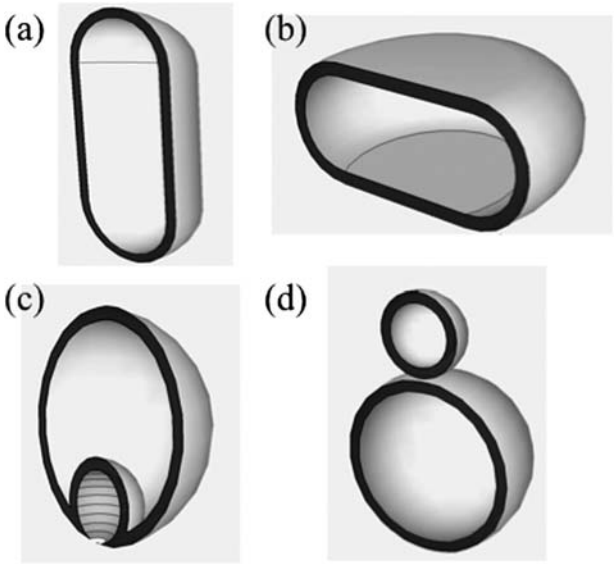

Fig. 3 Geometrical models (cross-section images) of (a) tube, (b) discocyte, (c) stomatocyte, and (d) twin vesicles. Dark grey region in the model indicates depletion zone covering the membrane surface with the thickness a (radius of colloid).

shapes, tube, discocyte, stomatocyte and multi-bead vesicles (Fig. 3). In order to obtain the excess area for tubular vesicles, we approximated the shape by a spherocylinder as shown in Fig. 3(a) and calculated the surface area A and the volume V. On the other hand, we obtained 3D image of the vesicle using confocal fluorescence microscope. From the 3D image, we measured the total surface area and volume. Then we compared the value of ξ defined by eqn (3) between the spherocylinder model and 3D image. The estimated degrees of deviation between the spherocylinder model and 3D image were ~10%. For the discocyte vesicle, we approximated the shape by a disk with round side (Fig. 3(b)) and the estimated degrees of the deviation were ~10% for $\xi = 0.1$ and ~17% for $\xi = 0.29$ (circular biconcave shape). For stomatocyte and twin vesicles, we approximated the shapes by the two spheroids as shown in Fig. 3(c) and (d). In these cases the degree of uncertainty originates from the uncertainty in measuring the radius of the spheroid, which is approximately 5%.

In Fig. 2(b) we plot the excess area as a function of time. The excess area increased monotonically until *ca.* 700 s and then reached a steady value of $\xi = 0.12$. Thus the shape deformation pathway is classified into two stages. In the first stage where the excess area increased monotonically, the GEDC deformed to the tubular vesicle using the excess area. This shape deformation pathway is consistent with the one observed in the vesicle without colloids. In the second stage where the vesicle kept the excess area constant, the GEDC showed the characteristic shape transition to the twin vesicle. The constant excess area indicates osmotic equilibrium between the inside and outside of the vesicle. Thus the shape deformation observed in the second stage is not caused by the osmotic pressure difference.[33] In this article we deal with the shape deformations of GEDC in the second stage.

In order to make clear the characteristic shape deformations of GV induced by the confinement of colloids, we mapped the shape

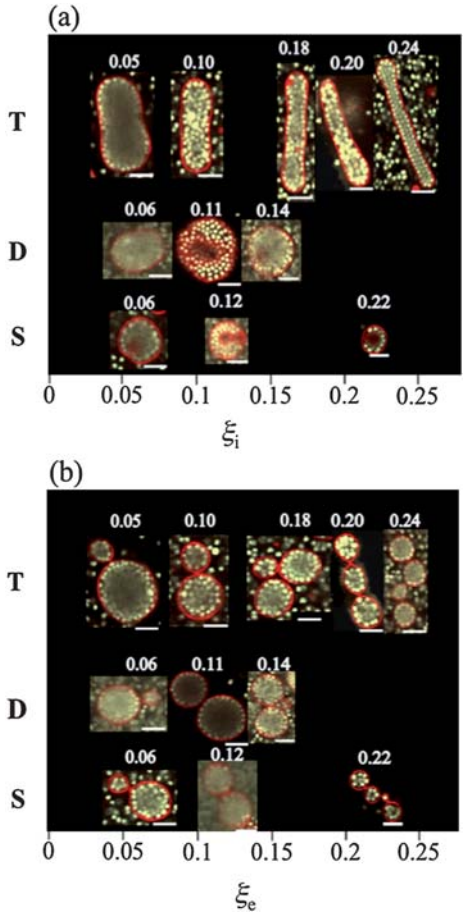

Fig. 4 (a) Tube (T), discocyte (D) and stomatocyte (S) GEDC shapes before the shape deformation as a function of the excess area at the initial point, ξ_i, and (b) GEDC shapes after the shape deformation from tube, discocyte, and stomatocyte. GEDCs as a function of excess area at the equilibrium point, ξ_e. Bar in each figure indicates 5 μm.

of the GEDC at the initial and the equilibrium points in the second stage against the excess area. We picked up three types of GEDCs, tube (T), discocyte (D), and stomatocyte (S). Fig. 4(a) shows the morphology diagram at the initial point in the second stage. For the estimation of the excess areas of the non-spherical GEDCs at the initial point, ξ_i, the tube, discocyte, and stomatocyte vesicles were approximated by spherocylinder, discocyte, and sphere in sphere geometries respectively. The calculated ξ_i is displayed at upper position of each photograph. These non-spherical GEDCs spontaneously deformed to the twins, triplets, and quadruplets of spheres, depending on the excess area of GEDCs. The equilibrium shapes of the GEDCs in Fig. 4(a) are mapped in Fig. 4(b). The excess area at the equilibrium point, ξ_e, was calculated by a sum of spheres (upper position). We plot the excess area of various GEDCs before the shape deformation, ξ_i, against that after the shape deformation, ξ_e, in Fig. 5. The data lie on a relation of $\xi_i = \xi_e$, indicating that the GEDC keeps the excess area constant during the characteristic deformation. Thus we concluded that the confined colloids induce the morphological transition of non-spherical vesicle to multi-bead vesicle.

We show a geometrical feature of the multi-bead vesicles. When we assume that the multi-beads vesicle is composed of

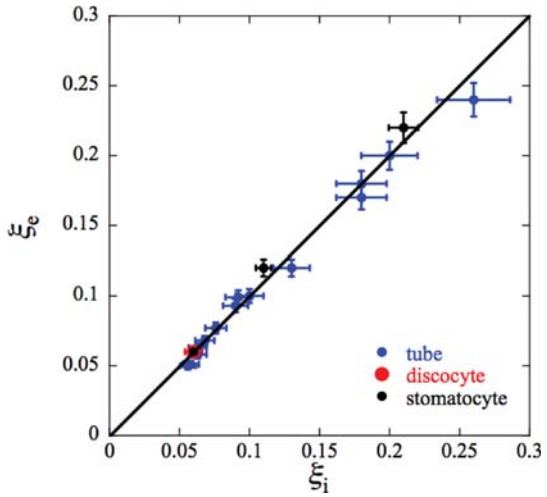

Fig. 5 Relationship between excess areas of GEDCs before (ξ_i) and after (ξ_e) the shape deformations. Data from tube, discocyte and stomatocyte vesicle are indicated by blue, red and black, respectively.

$n-1$ spheres with the radius R_{n-1} and one small sphere with radius R_1 ($R_1 < R_{n-1}$), the total area and volume of the multi-bead vesicle are expressed by

$$A = (n-1)4\pi R_{n-1}^2 + 4\pi R_1^2 \tag{4}$$

and

$$V = (n-1)\frac{4}{3}\pi R_{n-1}^3 + \frac{4}{3}\pi R_1^3 \tag{5}$$

respectively. Then we obtained a relation

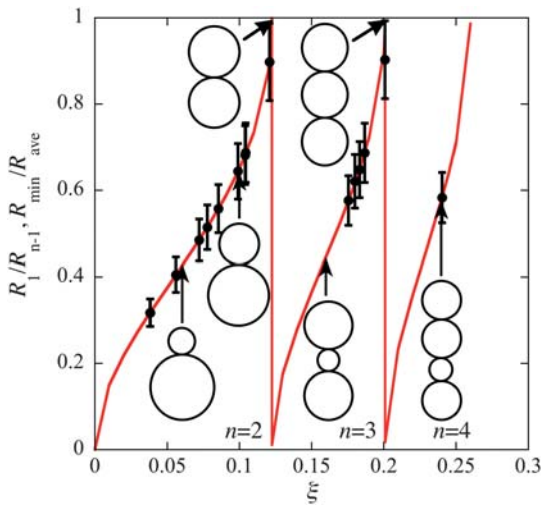

Fig. 6 Geometrical relationship between R_1/R_{n-1} and ξ predicted by eqn (6). Closed circle indicates the experimentally obtained ratio of the minimum sphere radius R_{min} to the averaged radius of other spheres R_{ave}^{n-1} in a multi-bead vesicle. Inset figures are schematic representations of multi-bead vesicles.

$$\xi = \frac{\left[(n-1) + (R_1/R_{n-1})^2\right]^{1/2}}{\left[(n-1) + (R_1/R_{n-1})^3\right]^{1/3}} - 1 \tag{6}$$

Fig. 6 shows the geometrical relation between R_1/R_{n-1} and ξ by a solid curve with schematic representations of multi-bead vesicles. In Fig. 6 we plot the ratio of the minimum sphere radius R_{min} to the averaged radius of other spheres R_{ave}^{n-1} in an observed multi-bead vesicle. We found good agreement between the experimental data and the geometrical prediction. Thus using the excess area of a non-spherical GEDC, the vesicle produces a small sphere on the mother spherical vesicle. With increasing excess area, the small vesicle increases its size. When the size of the second small sphere reaches to that of the mother vesicle, a third small sphere is produced. Then the multi-bead vesicle is composed of $n-1$ spheres with the same radius R_{n-1} and a remaining small sphere satisfying the geometrical constraint.

Shape deformation pathways

Here, we show the kinetic pathways of the shape deformations of GVs induced by the confinement of dense colloids. By encapsulating dense colloids inside of a short tubular GV with $\xi = 0.05$ (Fig. 7(a)), the tubular GV protruded a small spherical vesicle *via* a pear-like shape. The twin vesicle was connected by a very narrow neck and the confined colloids were homogeneously distributed in both spheres. For a discocyte GEDC with $\xi = 0.11$ (Fig. 7(b)), the discocyte protruded a part of the vesicle and deformed to a tubular vesicle (86 s). The tubular vesicle transformed to a twin vesicle in the same way as Fig. 7(a). A unique deformation was observed for the stomatocyte GEDC with $\xi = 0.12$ (Fig. 7(c)). In this case, the small empty vesicles inside of the vesicle were extruded and the stomatocyte vesicle deformed to a discocyte vesicle (28 s). The discocyte vesicle transformed to a twin spherical vesicle following the same pathway observed in Fig. 7(b). In Fig. 7(d) and (e) we show shape deformation pathways for the long tubular vesicles encapsulating dense colloids with $\xi > 0.12$, where GEDCs transformed to multi-bead vesicles with $n > 3$. The partitioning of the tubular vesicles started from the ends and the multi-bead vesicle satisfied the geometrical relation expressed by eqn (4) and (5), although for the very long tubular vesicles, the spheres are not so uniform (Fig. 7(e)).

Discussions

Here we discuss a mechanism of the multi-bead vesicle formation of the vesicle induced by the colloidal particles confinement. On the basis of the free energy expression for the vesicle encapsulating colloids expressed by eqn (1), the observed shape transition is caused by the membrane elasticity term or the confined charged colloid term. First we examine the contribution from the elastic energy term expressed by eqn (2), where a vesicle shape is determined by two parameters, the intrinsic area difference and the excess area. In this experiment, the GEDC keeps the excess area constant during the shape deformation as shown in Fig. 5. Thus the excess area is not responsible for the shape deformations. According to the morphology diagram based on the ADE model, the morphology transition from a tubular vesicle to

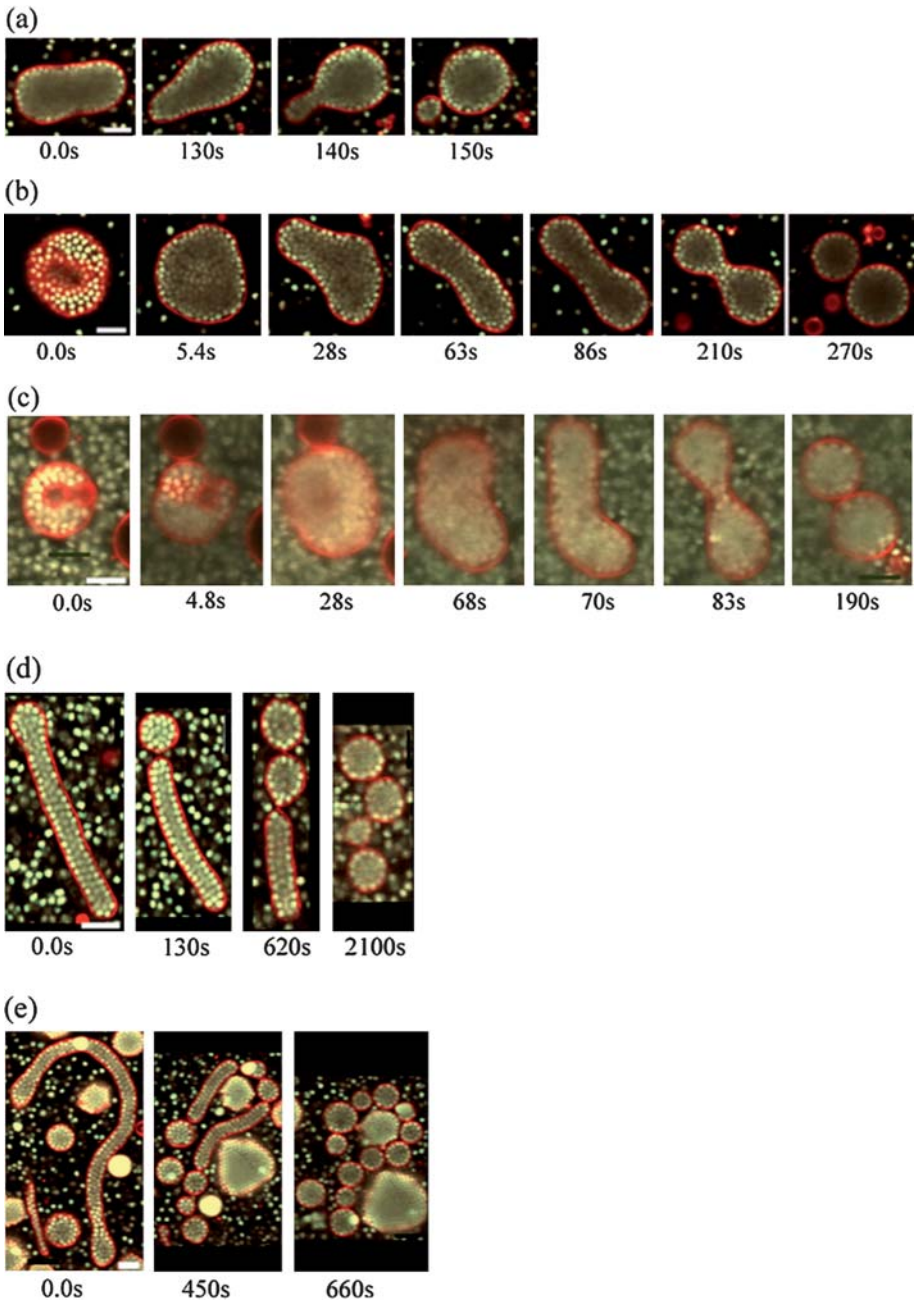

Fig. 7 Shape deformation pathways of GEDCs: (a) short tube ($\xi = 0.05$), (b) discocyte ($\xi = 0.11$), (c) stomatocyte ($\xi = 0.12$), (d) medium tube ($\xi = 0.24$), and (e) long tube ($\xi = 0.48$).

a twin vesicle is realized by the increase of the intrinsic area difference,[22–24] $\Delta A_0 = (N_{out} - N_{in})s_0$. In Fig. 8 we show the reduced area differences, $m \equiv \Delta A/[2t(A/4\pi)^{1/2}]$, expected for various vesicle shapes, tubular, discocyte, stomatocyte and twin vesicles as a function of the excess area. The twin vesicle has the largest area difference among the four vesicle shapes having the same excess area ξ. Thus when ΔA_0 of the vesicle is increased by the confinement of the colloids, the vesicle shape may transform to the twin vesicle shape. Generally vesicles keep the intrinsic area difference constant due to the extremely slow flip–flop motion.[34] However, if the lipids adsorb on the colloidal surface, the number of lipid molecules in the inner leaflet of the vesicle is decreased. This decrease leads to the increase of ΔA_0, which may cause the shape transformation to the twin vesicle.

We examined the adsorption of DOPC on colloid surface by a surface pressure measurement. To examine the adsorption of lipids on colloids, we equilibrated a fixed amount of DOPC lipids in a colloidal suspension with fractions of $\varphi_c = 0$, 0.02, and 0.10. If the lipids adsorb on the colloid surface, free DOPC molecules in the suspension should be decreased. This leads to decrease of the onset area, the surface area where the surface pressure–area profile starts to increase rapidly. The obtained normalized onset area, $S^{on}/S_0{}^{on}$ (S^{on}: onset area of the equilibrate DOPC in the colloid suspension and $S_0{}^{on}$: onset area of the pure DOPC), is

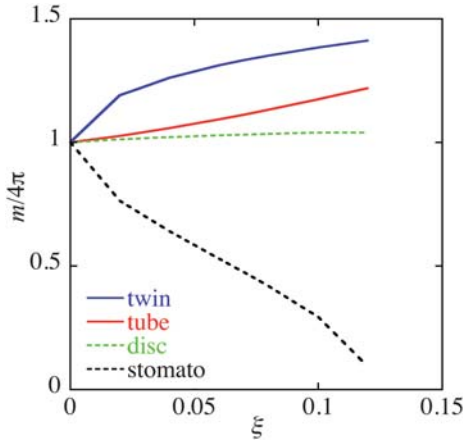

Fig. 8 Reduced area differences, $m \equiv \Delta A/[2t(A/4\pi)^{1/2}]$, expected for various vesicle shapes, tube, discocyte, stomatocyte and twin vesicles as a function of the excess area.

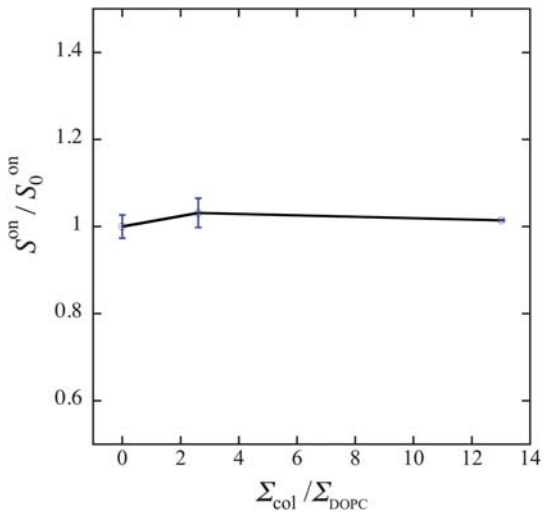

Fig. 9 Normalized onset area, S^{on}/S_0^{on}, in surface pressure–area isotherm against the ratio of total cross-section area of the DOPC lipids to the surface area of the colloids, $\Sigma_{col}/\Sigma_{DOPC}$.

plotted against the cross-section ratio ($\Sigma_{col}/\Sigma_{DOPC}$) in Fig. 9. The onset area did not depend on the colloid concentration, indicating that the number of adhering DOPC molecules on the colloid surface is negligible. Thus the number of lipid molecules in the inner leaflet does not change in the presence of the encapsulated colloids. We concluded that the elastic energy term is not responsible for the observed shape deformation.

Then the observed that multi-bead formation is caused by the confinement free energy term. For the negatively charged colloids, the encapsulated colloids prefer large free volume due to the electrostatic repulsive interactions. The free volume for the encapsulated colloids is expressed by $V_f = V - V_{dep}$, where V is the total volume of the vesicle and V_{dep} is the volume of the depletion zone covering the surface of the inner vesicle with the thickness of a. Since the vesicle kept the total volume constant during the deformation, the vesicle might deform so as to minimize the volume of the depletion zone. Here we compared the free volume of colloids encapsulated in four types of GVs having

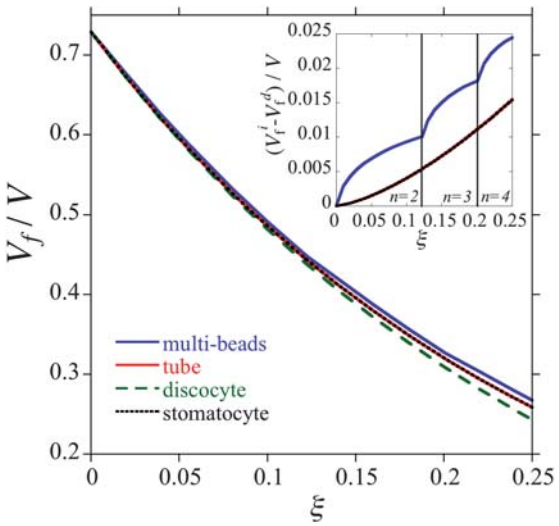

Fig. 10 Normalized free volume of twin, discocyte, tube, and stomatocyte vesicles as a function of the excess area. Free volume, V_f, is expressed by $V_f = V - V_{dep}$, where V is the total vesicle volume and V_{dep} is the volume of the depletion zone. Inset shows the free volume difference from the free volume of the discocyte vesicle, $(V_f^i - V_f^d)/V$, where V_f^i is the free volume of type i vesicle, i = multi-bead, tube and stomatocyte, and V_f^d is the free volume of the discocyte vesicle. Vertical lines at $\xi \approx 0.12$ and 0.20 indicate the transition excess area from $n = 2$ to 3 and $n = 3$ to 4, respectively.

the same volume, tube, discocyte, stomatocyte and multi-bead vesicles. The models for free volume calculation are schematically shown in Fig. 3, where the dark grey regions indicate the depletion zone covering the membrane surface. The obtained normalized free volumes, V_f/V, are plotted as a function of ξ in Fig. 10. In the inset we show the free volume difference from the free volume of the discocyte vesicle $(V_f^i - V_f^d)/V$, where V_f^i is the free volume of type i vesicle, i = multi-bead, tube and stomatocyte, and V_f^d is the free volume of the discocyte vesicle. The multi-bead vesicle has largest free volume among the four types of vesicles, $V_f^{multi\text{-}bead} > V_f^{tube}$, $V_f^{stomatocyte} > V_f^{discocyte}$, which is consistent with the observed deformations. Thus in order to minimize the free energy of the confined charged colloids, the GEDC deforms to the multi-bead vesicle. It should be noted that from the pure entropic free energy point of view, the partitioning of hard colloidal particles is unfavorable. For example, we consider the confinement free energy for two cases, one is that N colloids are confined in one container with volume V_1 and another one is that N colloids are confined two containers with the same volume V_2 ($2V_2 = V_1$). For the former case, the confinement free energy is expressed by $F_1^c = k_B TN\ln(N/V_1^c)$, where V_1^c is the free volume of colloids in a vesicle with volume V_1 and expressed by $V_1^c = V_1 - V_1^d$ (V_1^d: volume of the depletion zone). For the latter case, the confinement free energy is expressed by $F_2^c = k_B TN\ln(N/V_2^c)$, where V_2^c is the free volume of colloids in a vesicle with volume V_2. Since V_2^c is always smaller than V_1^c, we obtain $F_1^c < F_2^c$. Thus the repulsive inter-colloid interaction might be responsible for the observed shape transition to the multi-bead vesicle. Unfortunately to our knowledge, it is not clear whether the multi-spherical-bead vesicle has the largest free volume at a fixed vesicle volume or not, since it is a delicate mathematical problem to find

the vesicle shape giving the largest free volume by overlapping the depletion zone.

Conclusion

We confined charged colloid particles inside of the non-spherical vesicles. When the volume fraction of the encapsulated colloids is low ($\varphi_v < 0.03$), we could not find significant effects on the vesicle shapes, whereas for $\varphi_v \cong 0.5$, the vesicles with various shapes transformed to a multi-bead vesicle. The shape of the multi-bead vesicle is determined by geometrical constraints, conservations of total volume and total area of the vesicle. The multi-bead vesicle has largest free volume for the encapsulated colloids among other vesicle shapes examined in this study, tube, discocyte, and stomatocyte vesicles. This result strongly indicates that non-spherical vesicles deformed to the multi-bead vesicle to obtain largest free volume for the encapsulated colloids by overlapping the depletion zone on the inside of the vesicle surface. It should be noted that from the confinement entropy point of view, the partitioning of hard colloidal particles is unfavorable. While more experimental and theoretical works are necessary, the repulsive interaction between colloids might induce the observed transition.

Acknowledgements

We thank Prof. Takashi Taniguchi (Kyoto University) and Dr Miho Yanagisawa (Kyoto University) for valuable discussions. This work was supported by KAKENHI (Grant-in-Aid for Scientific Research) on Priority Area "Soft Matter Physics" from the Ministry of Education, Culture, Sports, Science and Technology of Japan and Grant-in-Aid for Scientific Research (B) 19340118 from Japan Society for the Promotion of Science.

References

1 S. Asakura and F. Oosawa, *J. Chem. Phys.*, 1954, **22**, 1255.
2 A. Vrij, *Pure Appl. Chem.*, 1976, **48**, 471.
3 V. J. Anderson and H. N. W. Lekkerkerker, *Nature*, 2002, **416**, 811.
4 P. B. Warren, *J. Phys. I*, 1994, **4**, 237.
5 M. Adams, Z. Dogic, S. L. Keller and S. Fraden, *Nature*, 1998, **393**, 349.
6 G. H. Koenderink, G. A. Vliegenthart, S. G. J. M. Kluijtmans, A. van Blaaderen, A. P. Philipse and H. N. W. Lekkerkerker, *Langmuir*, 1999, **15**, 4693.
7 Z. Dogic, D. Frenkel and S. Fraden, *Phys. Rev. E: Stat. Phys., Plasmas, Fluids, Relat. Interdiscip. Top.*, 2000, **62**, 3925.
8 K.-H. Lin, J. C. Crocker, A. C. Zeri and A. G. Yodh, *Phys. Rev. Lett.*, 2001, **87**, 088301.
9 A. Matsuyama and T. Kato, *Eur. Phys. J. E*, 2001, **6**, 15.
10 M. Imai, N. Urakami, A. Nakamura, R. Takada, R. Oikawa and Y. Sano, *Langmuir*, 2002, **18**, 9918.
11 M. Daoud and P. G. de Gennes, *J. Phys. (Paris)*, 1977, **38**, 85.
12 J. T. Brooks and M. E. Cates, *J. Chem. Phys.*, 1993, **99**, 5467.
13 C. Ligoure, G. Bouglet, G. Porte and O. Diat, *J. Phys. II*, 1997, **7**, 473.
14 L. Porcar, C. Ligoure and J. Marignan, *J. Phys. II*, 1997, **7**, 493.
15 G. Bouglet, C. Ligoure, A.-M. Bellocq, E. Dufoure and G. Mosser, *Phys. Rev. E: Stat. Phys., Plasmas, Fluids, Relat. Interdiscip. Top.*, 1998, **57**, 834.
16 V. Ponsinet and P. Fabre, *J. Phys. II*, 1996, **6**, 955.
17 M. Imai, R. Mawatari, K. Nakaya and S. Komura, *Eur. Phys. J. E*, 2004, **13**, 391.
18 P. Sens, M. S. Turnor and P. Pincus, *Phys. Rev. E: Stat. Phys., Plasmas, Fluids, Relat. Interdiscip. Top.*, 1997, **55**, 4394.
19 Y. Suganuma, M. Imai and K. Nakaya, *J. Appl. Crystallogr.*, 2007, **40**, s303–s306.
20 Y. Suganuma, N. Urakami, R. Mawatari, S. Komura, K. Nakaya-Yaegashi and M. Imai, *J. Chem. Phys.*, 2008, **129**, 134903.
21 K. Nakaya, M. Imai, S. Komura, T. Kawakatsu and N. Urakami, *Europhys. Lett.*, 2005, **71**, 494.
22 S. Svetina and B. Zeks, *Eur. Biophys. J.*, 1989, **17**, 101.
23 L. Miao, B. U. Seifert, M. Wortis and H.-G. Döbereiner, *Phys. Rev. E: Stat. Phys., Plasmas, Fluids, Relat. Interdiscip. Top.*, 1994, **49**, 5389.
24 U. Seifert, *Adv. Phys.*, 1997, **46**, 12.
25 B. Zoetekouw and R. van Roij, *Phys. Rev. E: Stat. Phys., Plasmas, Fluids, Relat. Interdiscip. Top.*, 2006, **73**, 021403.
26 C. Gögelein and R. Tuinier, *Eur. Phys. J. E*, 2008, **27**, 171.
27 A. V. Brukhno, T. Åkesson and B. Jönsson, *J. Phys. Chem. B*, 2009, **113**, 6766.
28 K. Tsumoto, H. Matsuo, M. Tomita and T. Yoshimura, *Colloids Surf., B*, 2009, **68**, 98.
29 H. I. Petrache, S. Tristram-Nagle, K. Gawrisch, D. Harries, V. A. Parsegian and J. F. Nagle, *Biophys. J.*, 2004, **86**, 1574.
30 H. Hotani, *J. Mol. Biol.*, 1984, **178**, 113.
31 M. Yanagisawa, M. Imai and T. Taniguchi, *Phys. Rev. Lett.*, 2008, **100**, 148102.
32 E. Boroske, M. Elwenspoek and W. Helfrich, *Biophys. J.*, 1981, **34**, 95.
33 R. Lipowsky and H.-G. Döbereiner, *Europhys. Lett.*, 1998, **43**, 219.
34 M. Nakano, M. Fukuda, T. Kudo, H. Endo and T. Handa, *Phys. Rev. Lett.*, 2007, **98**, 238101.

